Journal of Food Engineering 383 (2024) 112221

Contents lists available at ScienceDirect

Journal of Food Engineering

journal homepage: www.elsevier.com/locate/jfoodeng

Process intensification of microwave-assisted freeze-drying by frequency adjustment in real-time using solid-state technology

Till Kaysan *, Xiaoqi Zhou, Volker Gaukel

Institute of Process Engineering in Life Sciences, Food Process Engineering, Karlsruhe Institute of Technology, 76131 Karlsruhe, Germany

ARTICLE INFO

Keywords:
Freeze-drying
Microwaves
Frequency adjustment
Solid-state microwave technology
Process intensification

ABSTRACT

In microwave-assisted processes, solid-state microwave technology enables control of the electromagnetic field, which can be used for process intensification. This work investigates the impact of real-time frequency adjustment on microwave-assisted freeze-drying (MFD). Frequency-based control concepts were applied in experiments with tylose gel as a food model product in a laboratory-scale plant. By applying energy-efficient resonant frequencies based on feedback related to product state, the drying time was reduced by 24.2% compared to conventional freeze-drying (CFD) due to increases in energy efficiency. Comparable temperature profiles, residual moistures, and ascorbic acid retentions to CFD were achieved. However, structural degradation occurred with MFD in up to 10.4% of the samples. The degradation could be counteracted by more refined frequency and power application. In summary, this work demonstrates the high potential of frequency-based control for MFD process intensification.

1. Introduction

In process engineering, microwaves represent an alternative approach to energy supply, which can be used for process intensification. Contrary to convection, conduction, and thermal radiation in conventional thermal processing, the generation of heat via microwaves results from the interaction of the processed materials with an electromagnetic field (Thostenson and Chou, 1999). The respective dielectric properties characterize these interactions. Microwave application is associated with several advantages, such as selective heating, volumetric heating, and reduced process times (Clark and Sutton, 1996). In the context of food process engineering, the use of microwaves has been investigated for a variety of processes, such as freeze-drying (FD) (Ambros et al., 2018; Sickert et al., 2023b), vacuum drying (Drouzas et al., 1999; Dumpler and Moraru, 2023), heating (Kalinke et al., 2023; Taghian Dinani et al., 2021; Yang et al., 2022a), frying (Zhou et al., 2022), and defrosting (Yang and Chen, 2022).

In recent years, solid-state generators (SSGs) have emerged in the context of process engineering. Literature reports their use for the generation of microwaves in various microwave-assisted processes (Bianchi et al., 2017; Härdter et al., 2023; Hasegawa et al., 2017; Kalinke et al., 2023; Miyakawa et al., 2021; Tang et al., 2018; Tsubaki et al., 2020; Yang et al., 2023; Zhou et al., 2023). Unlike conventionally used magnetrons, SSGs allow precise control of the electromagnetic field by modulating the microwave power, microwave frequency, and phase shift between SSGs (Atuonwu and Tassou, 2018). The additional degrees of freedom in controlling the electromagnetic field can be used to optimize processes (Sickert et al., 2023a). Adjusting the frequency proved to be particularly promising in this context. Applying frequency sweeps enhanced heating uniformity in microwave-assisted heating processes (Antonio and Deam, 2005; Yang et al., 2019). More elaborate schemes of targeted frequency control, informed by preliminary experiments, resulted in enhanced energy efficiency (Kalinke et al., 2023; Yang et al., 2022a,b) and temperature homogeneity (Kalinke et al., 2023; Taghian Dinani et al., 2021; Yang et al., 2022a,b). High energy efficiency was achieved by applying individually energy-efficient frequencies and the excitation of multiple frequencies increased temperature homogeneity. In some studies, the frequencies were intentionally selected based on the corresponding heating pattern so that hot and cold spots would compensate each other during processing (Yang et al., 2022a,b). A trade-off between energy efficiency and temperature homogeneity was found when modulating the electromagnetic field (Bianchi et al., 2017; Yang et al., 2022a). Only one of the two parameters could be maximized. Some authors suggest control concepts to achieve a high performance regarding both parameters (Kalinke et al., 2023; Yang et al., 2022a). All of these control concepts for frequency are determined

* Corresponding author.
E-mail address: till.sickert@kit.edu (T. Kaysan).

https://doi.org/10.1016/j.jfoodeng.2024.112221
Received 2 December 2023; Received in revised form 30 June 2024; Accepted 6 July 2024
Available online 10 July 2024

before the start of the experiment. Therefore, the applied frequencies are not affected by any real-time feedback related to the product state.

The mentioned control concepts are limited in their applicability to processes where the product state undergoes significant changes over time, arising from the substantial effort required to base control concepts for these processes solely on prior experiments. The changes in product state occur mandatorily in microwave-assisted processes where phase transitions are an explicit goal, such as drying, defrosting, or pyrolysis. In these processes, a shift of frequencies with a local maximum in energy efficiency, so-called resonant frequencies (RFs), over process time was observed in monomodal cavities (Miyakawa et al., 2021; Tsubaki et al., 2020). These shifts were associated with changes in product state, presumably correlated with changing dielectric properties. Simulation-based preliminary work on microwave-assisted freeze-drying (MFD) in a multimodal cavity showed that multiple RFs shifted to higher frequencies (Sickert et al., 2023b). It is considered possible to increase both energy efficiency and power input homogeneity in MFD by applying multiple RFs, as it has been shown for microwave-assisted heating. The shifts in RFs, however, pose a challenge to their application throughout MFD, as frequency adjustment is required as a function of the product state. As far as the authors know, there has been no study of process control using frequency adjustment of RFs during the thermodynamically complex process of MFD based on real-time feedback related to product state. The approach would allow for targeted frequency adaption despite the substantial changes in product state. This extends the applicability of the approach to various processes and products without requiring excessive prior experiments.

This work investigates the effects of real-time frequency adjustment on the MFD process and selected product properties. The applied frequency-based control concepts are based on feedback related to the product state. The results are compared to conventional freeze-drying (CFD) as a benchmark. The experiments are conducted in a laboratory-scale dryer with tylose gel acting as a food model product. In MFD, microwave control is implemented using algorithms that adjust the microwave frequency based on product state. While focussing on control concepts with frequency adjustment during drying, control concepts with constant frequencies are also investigated as benchmarks. Targeted frequency adjustment is expected to increase energy efficiency throughout MFD, as shown for microwave-assisted heating. The resulting higher dissipated power may lead to an increase in product temperature and drying rate. Regarding product properties, there should be no discernible effect on residual moisture, provided that the termination criteria are selected appropriately for complete drying. Higher product temperature could lead to a decrease in thermally unstable compounds. Higher dissipated microwave power above a threshold is expected to cause more macroscopic impairment of the product, as observed in previous work for the initial stage of MFD (Sickert et al., 2023a).

2. Materials and methods

2.1. Model product

Tylose gel cuboids with ascorbic acid (AA) as a tracer substance served as a food model product. The sample preparation was identical to the procedure described in a previous paper (Sickert et al., 2023b). In brief, tylose gel composed of 76.23 wt% demineralized water, 23.77 wt % tylose MH1000 (Kremer Pigmente, Aichstetten, Germany), and 1.00 wt% L-(+)-AA (Carl Roth, Karlsruhe, Germany) was produced. Then, cuboids of tylose gel were molded in dimensions of around 25 mm × 25 mm × 10 mm with a weight of 12.50 ± 0.05 g each and frozen at −30 °C for a minimum of 14 h.

2.2. Freeze-drying system

Fig. 1 shows a schematic view of the laboratory-scale FD system and a depiction of the process chamber. The stainless steel process chamber had inner dimensions of 612 mm × 400 mm × 300 mm. A custom-made cold trap (UCCT, Vienna, Austria) and a NEO D 65 vacuum pump (Leybold, Cologne, Germany) were connected in series to the process chamber. The cold trap temperature and the chamber pressure were set to −60 °C and 0.5 mbar in all experiments. An HY2020 SSG (TRUMPF, Freiburg, Germany) was connected via a coaxial cable to a waveguide port centrally embedded in the top of the process chamber. The SSG could generate microwaves of up to 600 W in power and frequencies from 2400 MHz to 2500 MHz at intervals of 0.01 MHz. Based on qualitatively validated electromagnetic simulations, we inferred a relatively uniform distribution of the power associated with the dissipation of the electromagnetic field among the tylose samples, particularly when multiple frequencies are applied (Sickert et al., 2023b). For CFD, a custom-built modular heat exchanger was placed in the process chamber as a product support. An AC200 thermostat (Thermo Fisher Scientific, Henningsdorf, Germany) could be set to −5 °C to 70 °C to regulate shelf temperature. The sensors used were a CMR363 capacitive pressure sensor (Pfeiffer, Aβlar, Germany), three FOS-TG fiber optic temperature sensors (Rugged Monitoring, Quebec, Canada), and a PW4MC3/2 kg load cell (Hottinger Brüel & Kjaer, Darmstadt, Germany). Moreover, the internal sensors of the SSG for forward power and reflected power were used. The PW4MC3/2 kg load cell was connected to a product support made of polyether ether ketone, which was placed centrally at the bottom of the process chamber and could be used for MFD only. Scripts in Matlab 2020b (MathWorks, Natick, USA) were used to store the recorded process parameters and control the power and frequency of the microwaves throughout drying.

Calibration was performed for all sensors. FOS-TG sensors underwent three-point calibrations using a Pt-25 platinum resistance

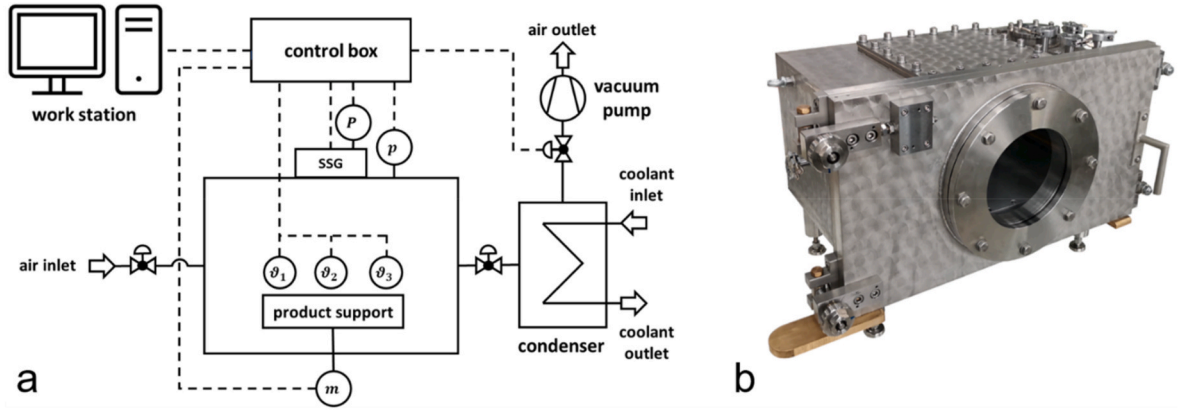

Fig. 1. (a) Schematic representation of the laboratory-scale MFD setup. m – load cell, P – sensor microwave power, p – capacitive pressure sensor, ϑ_i – fiber optic temperature sensors. (b) Process chamber with no peripheral devices connected.

thermometer MKT25 (Rosemount, Shakopee, USA). The PW4MC3/2 kg load cell was calibrated using calibration weights, covering product weights up to 300 g. The SSG and the CMR363 pressure sensor were acquired in a calibrated state during the construction of the system.

2.3. Process characterization

Process characterization of MFD was conducted to determine the initial RFs. RFs are defined here as the frequencies with a local maximum in energy efficiency. Twenty-four frozen cuboids of tylose gel were placed centrally on the product support with a spacing of 5 mm, as depicted in Fig. 2. Fiber optic temperature sensors were positioned centrally in samples 4, 6, and 10, in which holes were drilled during sample preparation. Subsequently, the process chamber was sealed airtight and the valve to the vacuum pump was opened. The application of microwaves started 10 min after the vacuum application. A frequency sweep in the range of 2400 MHz to 2500 MHz was performed with an interval of 0.1 MHz and the minimally feasible set forward power of 50 W. From the reflected power P_r and forward power P_f monitored by the SSG, the energy efficiency η was calculated by $\eta = 1 - P_r / P_f$. The results of an exemplary frequency sweep are shown on the left in Fig. 3. All process characterizations were repeated three times. The final RFs were calculated as the arithmetic means of the three RFs obtained.

2.4. Drying procedure

For MFD, the starting procedure and the placement of samples were identical to the process characterization described in Section 2.3. The application of microwaves marked the start of the process time. The process specifications set for all experiments were a forward power of 50 W and an activation ratio of 0.5. The latter describes the time ratio the SSG was active when applying each frequency for 10 s. When multiple frequencies were used, the frequencies were applied in a loop in ascending order. The following frequency-based control concepts were investigated.

- Single Constant Frequency (1CF) – constant frequency of 2420 MHz,
- Six Equidistant Frequencies (6EF) – six constant frequencies from 2400 MHz to 2500 MHz in an interval of 20 MHz,
- Six Minimum Resonant Frequencies ($6RF_{min}$) – six RFs displaying the lowest energy efficiencies, purposefully adjusted during MFD, and
- Six Maximum Resonant Frequencies ($6RF_{max}$) – six RFs displaying the highest energy efficiencies, purposefully adjusted during MFD.

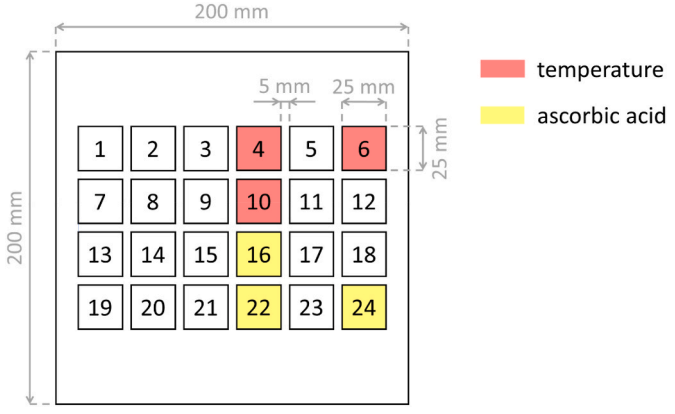

Fig. 2. Placement of samples on product support for MFD. Samples equipped with fiber optic temperature sensors are marked in red and samples for determination of ascorbic acid content are marked in yellow. The samples in the bottom row are adjacent to the front door of the process chamber. The samples were placed centrally on the heat exchanger in the same arrangement for CFD.

The primary focus of the investigations was on the control concepts $6RF_{min}$ and $6RF_{max}$, which implemented real-time modulation of the microwave frequency based on the product state. Previous electromagnetic simulations have demonstrated the potential benefits of similar control concepts based on applying multiple RFs (Sickert et al., 2023b). The remaining control concepts, 1CF and 6EF, maintained constant frequencies throughout the drying process, allowing comparisons with benchmark processes. Specifically, 6EF was selected for its equivalence in the number of applied frequencies to $6RF_{min}$ and $6RF_{max}$, while 1CF represents the most straightforward application of microwave frequency. Furthermore, the substantial difference in energy efficiency between $6RF_{min}$ and $6RF_{max}$ enabled the assessment of the impact on energy efficiency or dissipated power within the control concepts employing real-time frequency modulation. MFD was terminated when the drying rate $\dot{m}$ was less than 0.25 g/h, calculated over 1 h.

The specifications for CFD were established in preliminary experiments using the criteria of complete and fast drying without compromising product quality. The thermostat temperature was initially set to −5 °C as the minimally viable temperature to prevent the melting of the samples due to contact with the hot shelf. The samples were placed centrally on the heat exchanger with the sample and temperature sensor positions shown in Fig. 2. Following a vacuum application for 10 min, the thermostat was set to 70 °C, indicating the start of the process time. When all temperature sensors reached a temperature difference of less than 2 K/h over 20 min, the process was extended by 20% of the current process duration before termination. All drying experiments were conducted at least in duplicate.

2.5. Control algorithm frequency

The applied frequency-based control concepts can be subdivided into control concepts with constant frequencies, 1CF and 6EF, and concepts with frequency adjustment throughout drying, $6RF_{min}$ and $6RF_{max}$. An approach to real-time frequency adjustment was developed for $6RF_{min}$ and $6RF_{max}$ to enable the frequent update of RFs throughout drying in a time-saving manner. The concept is based on the shift of RFs to higher frequencies during MFD (Sickert et al., 2023b) and is depicted schematically in Fig. 3. The initial RFs, as determined in process characterization, were provided as inputs to the control algorithm. At the beginning of the process, the frequency range around all RFs was screened locally for maximum energy efficiency. The range was −0.5 MHz to +0.5 MHz around each RF at an interval of 0.1 MHz. The frequencies of maximum energy efficiency were stored as the new RFs. Subsequently, the most recent RFs were selected for the drying process. The six RFs with the lowest energy efficiency were applied for the control concept $6RF_{min}$, while the six RFs with the highest energy efficiency were used for $6RF_{max}$. Every 20 min, the screening and application of updated RFs were repeated analogously to the beginning of the process.

2.6. Sample analysis

2.6.1. Structure

An X-ray microscope Xradia 520 Versa (Carl Zeiss, Oberkochen, Germany) was employed to visualize the sample structure in μ-CT. Details on the microscope, the schematic experimental setup, and the principles of μ-CT can be found in the literature (Straube et al., 2021). Exemplary specimens of intact and impaired samples were placed on the sample holder. For image capture, the imaging mode was set to tomography, the optical magnification to 0.4, the exposure time to 1 s, and the binning to 1. The source settings for voltage and power were 80 kV and 2 W, respectively.

2.6.2. Residual moisture

The weights of the samples after drying m_{FD} were determined using a balance type 1518 (Sartorius, Göttingen, Germany). Following FD, the

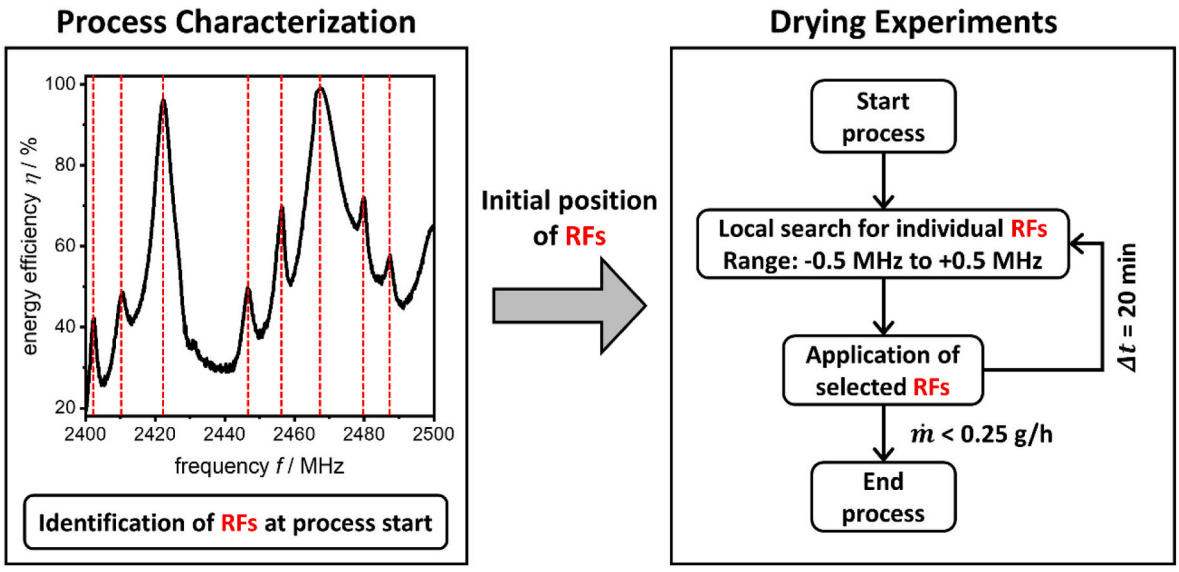

Fig. 3. Flowchart of frequency adjustment during MFD experiments in the context of process characterization.

samples were cut in half and examined for macroscopic structural impairment. Samples 16, 22, and 24 were set aside for later determination of AA retention. The remaining samples were placed in a T6060 drying oven (Heraeus, Hanau, Germany) at 105 °C for at least 24 h. Subsequently, the samples were weighed using an LS 220A SCS precision balance (Precisa, Dietikon, Switzerland). The respective weight was used as the dry mass m_{dry} to calculate the dry basis residual moisture X_{res} with $X_{res} = (m_{MFD} - m_{dry})/m_{dry}$.

2.6.3. Ascorbic acid retention

Analysis of AA retention was performed according to Ballentine (1941). For this purpose, samples 16, 22, and 24 were ground using a coffee grinder M 55 (Petra Deutschland, Ense, Germany) and then classified with a sieve into particles smaller than 1 mm. A Precisa LS 220A SCS precision balance was used to weigh a sample mass corresponding to 0.013 g AA in the undried state. The weighed sample was mixed with 50 mL of double-distilled water and stirred for 30 min at 200 rpm using a PC-420D magnetic stirrer (Corning, Corning, USA). The resulting suspension was homogenized with an ULTRA-TURRAX T 25 (IKA-Werke, Staufen im Breisgau, Germany) using an S 25 N - 18 G dispersing tool (IKA-Werke, Staufen im Breisgau, Germany) at 5000 rpm for 2 min. Subsequently, 2 mL of a 1 wt% starch solution (Carl Roth, Karlsruhe, Germany), 2 mL of a 2-M potassium iodide solution (Carl Roth, Karlsruhe, Germany), and 6 mL of 1-M sulfuric acid were added. The mixture was stirred at 280 rpm with a magnetic stirrer, while a 0.001-M potassium iodate solution (Carl Roth, Karlsruhe, Germany) was titrated dropwise until the equivalence point was reached. This was reflected by a color change of the liquid to red-violet. The titration volume was converted into the corresponding mass m_{AA} and retention $m_{AA}/m_{AA,0}$ of AA using the equation $m_{AA} = 3V_{IO_3^-}c_{IO_3^-}\widetilde{M}_{AA}$. Here, $V_{IO_3^-}$ and $c_{IO_3^-}$ are the volume and molar concentration of the iodate solution, while $\widetilde{M}_{AA}$ is the molar mass of AA. The initial mass of AA $m_{AA,0}$ was calculated from the mass of the weighed sample and the composition of the tylose gel. Since the potassium iodide solution is sensitive to light, it had to be prepared immediately before the experiment and then shielded from light. The determination was done in triplicate for each sample.

3. Results and discussion

3.1. Influence of frequency control on MFD

3.1.1. Energy

Targeted frequency application in microwave-assisted heating increased energy efficiency, resulting in a higher average product temperature (Kalinke et al., 2023). For the initial stage of MFD, targeted frequency application was linked to increased energy efficiency (Sickert et al., 2023a). Fig. 4a shows the energy efficiency as a function of time to evaluate the transferability of these results to complete MFD. In all experiments, energy efficiency tended to decrease during drying. Applying $6RF_{max}$ and $6RF_{min}$ yielded the highest energy efficiencies throughout drying, averaging 64.63% and 43.62%, respectively. The 6EF and 1CF control concepts followed in descending order with 40.12% and 37.49%, respectively. Targeted application of frequencies by real-time adjustment throughout MFD with $6RF_{max}$ led to an absolute increase in energy efficiency of 24.51% compared to 6EF. With 6EF, the same number of frequencies was applied but kept constant throughout drying.

Periodic jumps in energy efficiency occurred for the control concepts with frequency adjustment, $6RF_{min}$ and $6RF_{max}$. The jumps occurred at intervals of 20 min, immediately after the search for RFs. While relatively small jumps are probably caused by slight frequency adjustments, more pronounced jumps are related to applying a modified set of RFs. The latter occurred when local maxima in energy efficiency were lost or redetected around previously applied RFs. The replacement of previously applied RFs with different RFs of notably higher or lower energy efficiency presumably led to the more pronounced jumps in energy efficiency.

Fig. 4b shows the average energy efficiency as a function of dry basis moisture to emphasize the dependence of energy efficiency on product state. Using $6RF_{max}$ generally resulted in the highest energy efficiency throughout MFD, particularly at a moisture content of less than 2.5 g/g. On the other hand, the overall energy efficiency reached by $6RF_{min}$ was similar to those of control concepts without frequency adjustment.

A comparison of $6RF_{max}$ and $6RF_{min}$ shows that RF application can adjust the energy efficiency over a wide range throughout the drying process. This is particularly advantageous at low moisture content towards the end of drying. At this stage, energy efficiency is lowest when constant frequencies are used in 1CF and 6EF. The particularly low energy efficiency is probably due to the low dielectric properties of the dried tylose gel compared to the frozen state (Sickert et al., 2023b). The

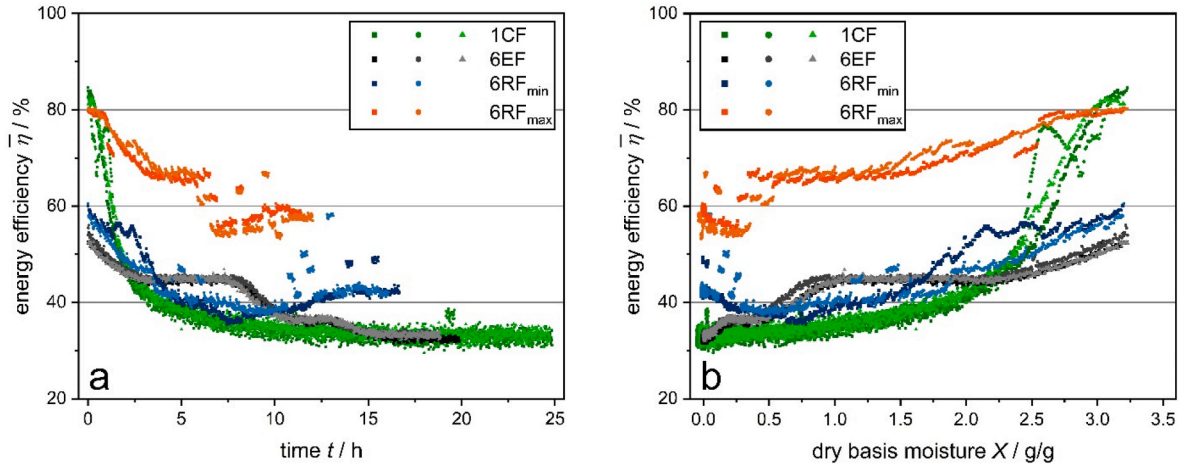

Fig. 4. (a) Energy efficiency as a function of process time for the applied control concepts in MFD. (b) Energy efficiency as a function of dry basis moisture. The energy efficiency of the frequency loops in 6EF, 6RF$_{min}$, and 6RF$_{max}$ was calculated as the average of the individual frequencies.

flexible solid-state technology may be used in further fine-tuning to adjust the energy efficiency between the values of 6RF$_{min}$ and 6RF$_{max}$ intentionally using different combinations of RFs. For example, using the highest possible number of RFs may result in a highly uniform drying process. Further increases in energy efficiency are also possible by higher weighting of highly energy-efficient RFs via a more prolonged activation of these frequencies.

Compared to the average energy efficiency of 43.6% of MFD with 6RF$_{min}$, the process with 6EF reached a similar value of 40.1%. This corresponds to a relative deviation of 8.7%. Process duration varied between 16.32 h for the 6RF$_{min}$ process and 18.97 h for the 6EF process, corresponding to a deviation of 14.0% (see Section 3.1.3). This discrepancy can be explained partly by varying forward powers at different frequencies since multiplying forward power by energy efficiency gives the dissipated power. Literature shows the correlation of the dissipated power with the heating power in microwave-assisted heating (Wang et al., 2015) and with the drying kinetics in MFD (Sickert et al., 2023a). Unfortunately, the SSG used delivered a frequency-dependent forward power, contributing to different power dissipation in the experiments. Fig. 5 shows the dissipated power nominated to the sample weight at the start of MFD in dependence on process time. The differences in the relative positions among the experiments between Figs. 5 and 4a can be attributed to variations in forward power during the experiments. Aside from energy efficiency, forward power is the sole parameter influencing dissipated power (see Section 2.3).

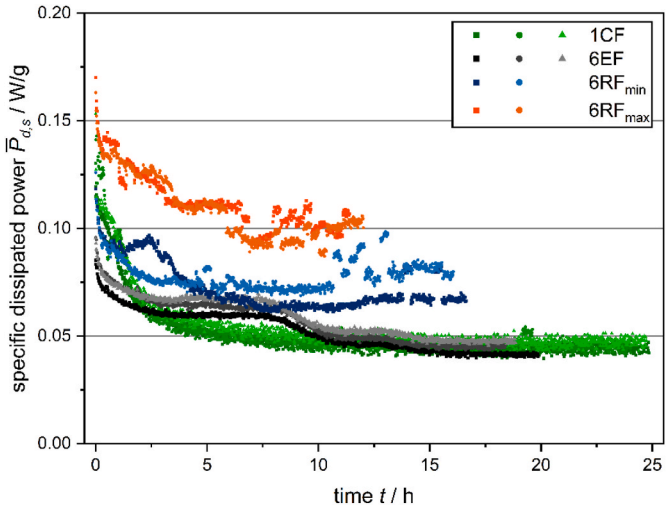

Fig. 5. Dissipated power standardized to the sample mass at the start of MFD as a function of process time for the applied control concepts in MFD. The specific dissipated power of the frequency loops in 6EF, 6RF$_{min}$, and 6RF$_{max}$ was calculated as the average of the individual frequencies.

To further investigate the interactions among microwave parameters, Table 1 lists the average specific forward power, average energy efficiency, and average specific dissipated power for all experiments. Both specific dissipated power and energy efficiency vary for the control concepts. The specific forward power is comparable between 1CF and 6EF and between 6RF$_{min}$ and 6RF$_{max}$. Consequently, the difference in forward power must be considered when analyzing the impact on the process, especially when comparing the two groups of adjusted and non-adjusted control concepts. For instance, the different process durations of 6RF$_{min}$ and 6EF at similar energy efficiency are caused by differences in the forward power. Despite these limitations, the apparent difference in energy efficiency between 6RF$_{max}$ and the remaining control concepts reveals that microwave frequency influences the conversion of electromagnetic energy into heat, thereby affecting the drying process.

3.1.2. Sample temperature

Higher dissipated microwave power is expected to lead to increased temperatures of the samples. Fig. 6 shows the temperature of sample 6 in the corner of the arrangement (see Fig. 2) as a function of process time. Sample 6 was chosen, as this sample reached the highest temperature of samples 4, 6, and 10, as depicted in Fig. A1 in the Appendix. The presumable cause is thermal radiation from the walls of the process chamber, as was indicated in previous work (Sickert et al., 2023a). Only one experiment of each process is shown for the sake of clarity. Fig. A2 in the Appendix shows the reproducibility of the temperature curves. The samples in CFD showed the most considerable deviations among experimental repetitions, presumably due to the varying contact area between the slightly uneven samples and the heat exchanger. The

Table 1
Average values of the microwave-related process parameters of all MFD experiments. The parameters were averaged over all frequencies and the entire process time.

Control Concept	Average Specific Forward Power $\overline{P}_{f,s,proc}$/W/g	Average Energy Efficiency $\overline{\eta}_{proc}$/%	Average Specific Dissipated Power $\overline{P}_{d,s,proc}$/W/g
1CF	0.135; 0.137; 0.143	37.1; 37.6; 37.7	0.050; 0.052; 0.054
6EF	0.126; 0.133; 0.140	39.6; 40.8; 40.1	0.052; 0.057; 0.059
6RF$_{min}$	0.173; 0.188	43.3; 44.0	0.073; 0.079
6RF$_{max}$	0.181; 0.180	64.9; 64.3	0.112; 0.109

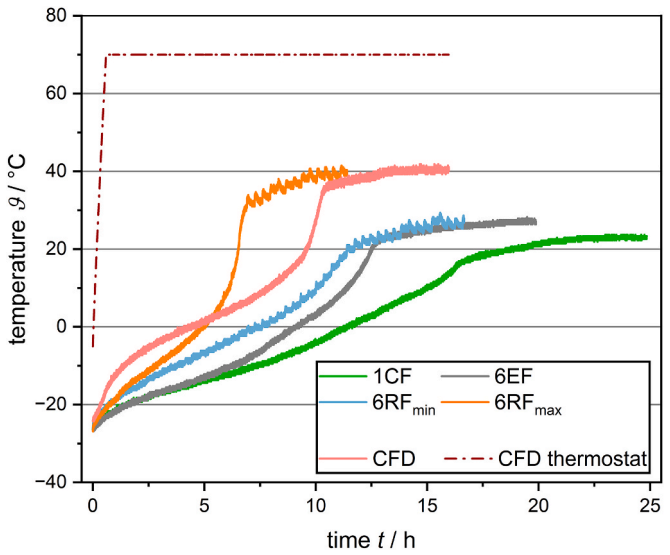

Fig. 6. Temperature of sample 6 as a function of process time for MFD and CFD experiments. One experiment is shown for each process. The solid lines mark the temperatures measured inside the samples. The dash-dotted line marks the thermostat temperature in CFD.

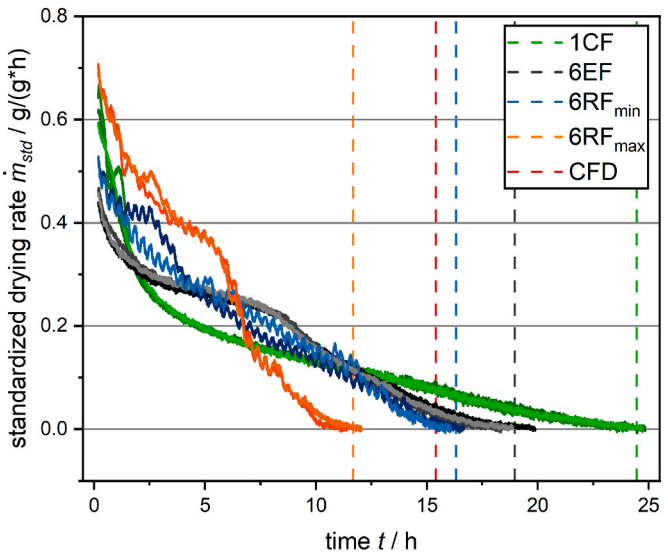

Fig. 7. Drying rate standardized to the dry mass of the samples as a function of the process time of MFD for the applied frequency-based control concepts. Dashed lines mark the average duration of the drying process for MFD and CFD, while solid lines in the corresponding colors show the respective drying kinetics.

temperature curves are typical for MFD (Ambros et al., 2018; Härdter et al., 2023). The temperature initially increases relatively quickly as soon as microwave power is applied. A phase of slowly increasing temperature follows due to the energy required to supply the latent enthalpy of sublimation. After that, the rate of temperature change increases, as the decreasing sublimation requires less energy before the dry samples reach an equilibrium temperature. In this state, the dissipated microwave power and heat losses due to thermal radiation and conduction are approximately equivalent.

Periodic temperature jumps were observed when the frequencies were adjusted in $6RF_{min}$ or $6RF_{max}$, mirroring the observed jumps in energy efficiency. Therefore, the increase in energy efficiency led to a higher power loss inside the samples – the power was not just dissipated elsewhere, e.g., in the coaxial cable or as wall losses.

The dissipated power, standardized to the mass of the samples at the start of MFD and averaged over the respective experiments, increases in the order of 1CF, 6EF, $6RF_{min}$, and $6RF_{max}$ and amounts to 0.052 W/g, 0.056 W/g, 0.076 W/g, and 0.111 W/g, respectively. Following expectations, higher specific power dissipation correlated with higher product temperature throughout MFD, as shown in Fig. 6. The maximum sample temperatures of all MFD experiments were 23.7 °C, 29.0 °C, 33.6 °C, and 43.8 °C for 1CF, 6EF, $6RF_{min}$, and $6RF_{max}$, respectively. Hence, maximum temperature is also correlated with specific dissipated power. However, the maximum temperature occurred in the final phase of MFD in all experiments. Therefore, it is expected only to be influenced by the power dissipation at this stage. The maximum temperature for CFD was 44.0 °C, slightly higher than the 43.8 °C for MFD with $6RF_{max}$. Thus, heat-sensitive products can be treated with both CFD and MFD due to a similar temperature stress. Final drying at lower temperatures becomes feasible when the specific dissipated power is reduced at this stage, as evidenced by the behavior observed with the other MFD control concepts.

3.1.3. Drying kinetics

An increase in power dissipation is expected to result in higher drying rates during MFD, as observed for its initial stage (Sickert et al., 2023a). The assumption underlying this dependence is that the process is at least partly limited by heat transfer. Fig. 7 illustrates the drying rate normalized to the dry mass of the samples over time. All kinetics show the highest drying rate in the initial stages, followed by a decline over process time. This drying kinetics behavior is qualitatively consistent with the MFD of banana slices (Jiang et al., 2013) and lactic acid bacteria (Ambros et al., 2018).

As expected, $6RF_{max}$ shows the highest drying rates, as it is the process with the highest average specific dissipated power (see Table 1). The dotted lines in Fig. 7 indicate the process duration at which MFD and CFD termination criteria were met. Completion of CFD took 15.41 h on average. The only MFD process with a shorter duration was $6RF_{max}$ at 11.68 h. 1CF, 6EF, and $6RF_{min}$ resulted in longer durations of 24.47 h, 18.97 h, and 16.32 h, respectively. Consequently, $6RF_{max}$ reduced process time by 24.2% compared to CFD and 38.4% compared to 6EF, where the same number of frequencies was applied but kept constant throughout drying. Thus, MFD was successfully intensified via frequency modulation to reach drying times below the benchmark process of CFD.

The periodic jumps in drying rate for $6RF_{max}$ and $6RF_{min}$ indicate that the increased energy efficiency with each frequency adjustment directly translated into an increase in mass transfer. The relationship between energy efficiency, product temperature, and drying rate based on the reoccurring fluctuations of all three parameters with frequency adjustment every 20 min is apparent. In the literature, higher sample temperatures in MFD can also be associated with a higher drying rate (Ambros et al., 2018).

3.2. Influence of frequency control on product properties

3.2.1. Structure

Previous work on partial MFD revealed structural impairments in some samples (Sickert et al., 2023a). Complete MFD in this work led to the same effect in several samples. Fig. 8a shows tomographic images of exemplary samples with and without structural impairment. In the following, these are referred to as intact and puffed. The term puffed in this context refers to the inner structure of the samples. The sample volume is not influenced by puffing. The intact sample shows the typical lamellar structure of a freeze-dried product, as detected in carrots (Siebert et al., 2020). The same lamellar structure is visible in the outer layer of the puffed sample. In contrast, the interior of the puffed sample is characterized by relatively large pores with optically dense structures in between, typical of puffed products, e.g., puffed rice (Gulati and

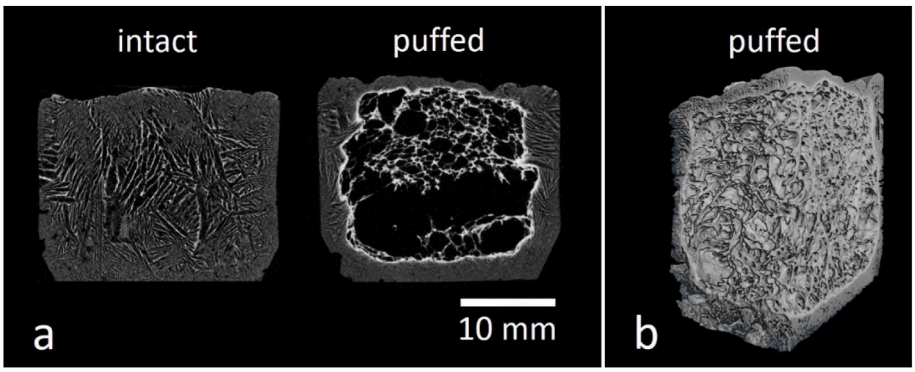

Fig. 8. (a) Tomographic images of dried tylose gel samples in the intact and puffed state. (b) Segment from the 3D reconstruction of a puffed tylose gel sample.

Datta, 2016). Fig. 8b displays a 3D segment of the puffed sample, illustrating the structural variances within the sample.

The puffed structure is probably caused by the melting of frozen water in individual samples due to high dissipated microwave power during MFD. The emergence of liquid water leads to even higher dissipated power in the samples since it has relatively high dielectric properties compared to ice. This effect is reflected by the jump in energy efficiency during one MFD experiment with 1CF at a moisture content of about 2.5 g/g, possibly due to a melted sample (see Fig. 4b). Accordingly, the drying rate in this experiment increased (see Fig. 7) and puffing with 1CF occurred only in this experiment. The resulting increase in vapor pressure inside the sample probably caused the formation of the large pores. The same principle of sudden evaporation and expansion of water inside the material is used in explosion puffing drying, which results in a similar structure (Zou et al., 2013). In the present work, the freeze-dried outer layer was too rigid to be affected by the pressure gradient. Consequently, the volume was not increased. Only the structure of the inner thawed layer was affected before the vapor could escape and drying progressed.

The ratios of puffed samples from CFD and MFD are shown in Table 2. There was no puffing in CFD, whereas puffing occurred in at least one MFD experiment for each control concept. Drying with $6RF_{max}$ resulted in the highest average puffed sample ratio of 10.4%, with puffing occurring in every experiment. The results are consistent with the proposed mechanism for puffing, as $6RF_{max}$ also exhibits the highest average dissipated specific power (see Table 1). The puffing of the samples was reduced when RFs with lower energy efficiency were applied in $6RF_{min}$. Puffing may also be reduced by varying the weights of individual frequencies applied or reducing the microwave power. However, these measures are likely to involve trade-offs regarding process performance.

3.2.2. Residual moisture

If similar air humidity is assumed, all samples should have similar residual moisture content after drying. Fig. 9 provides an overview of the dry basis residual moisture for the individual samples from all FD processes. The residual moisture of all samples is below 0.020 g/g except for one sample from 6EF, in which moisture is 0.029 g/g. The residual moisture ranges without statistical outlieres are relatively similar for all processes, ranging from 0.005 g/g to 0.012 g/g with $6RF_{max}$ up to 0.004 g/g to 0.018 g/g with 1CF. The overlaps in the ranges of all processes indicate similar product stabilities for samples processed with CFD and MFD. The obtained values of residual moisture are comparable to those in the literature. These are dry basis residual moistures for CFD of strawberries of minimally 0.00 g/g to 0.01 g/g (Shishehgarha et al., 2002), around 0.05 g/g for MFD of apple chips (Huang et al., 2011), approximately 0.005 g/g to 0.025 g/g for MFD of various pharmaceutical model formulations (Härdter et al., 2023), and the targeted value of 0.048 g/g for starter cultures (Ambros et al., 2018).

Even though there are no notable differences in residual moisture among the control concepts, there seem to be deviations between the experiments for individual control concepts. These deviations are particularly apparent for 1CF, where the residual moistures of two experiments are clustered around 0.013 g/g and the residual moistures of the third experiment are clustered around 0.005 g/g. The accumulations might be caused by air humidity fluctuations or puffing in the experiment with lower residual moisture. However, the residual moisture of puffed samples did not systematically deviate from the values of intact samples, as observed in the samples from $6RF_{max}$. Only one puffed sample at 6EF shows a much higher residual moisture than its intact counterparts.

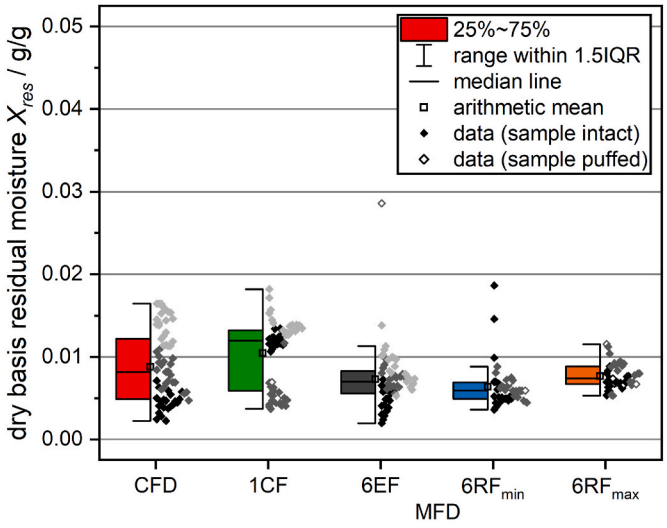

Fig. 9. Dry basis residual moisture of samples from CFD and MFD with the applied control concepts. The samples of each experiment within the various processes are shown in a different shade of gray.

Table 2
Ratio and average ratio of puffed samples of all FD experiments. One occurrence of puffing in 24 samples corresponds to a puffed sample ratio of approximately 4.2%.

Process	CFD	MFD 1CF	MFD 6EF	MFD $6RF_{min}$	MFD $6RF_{max}$
Puffed Sample Ratio y/%	0.0; 0.0; 0.0	0.0; 8.3; 0.0	0.0; 4.2; 0.0	8.3; 4.2	12.5; 8.3
Average Puffed Sample Ratio $\bar{y}$/%	0.0	2.8	1.4	4.2	10.4

3.2.3. Ascorbic acid retention

Higher product temperature could decrease AA content, as AA is a typical heat-sensitive nutrient (Saguy et al., 1978). Fig. 10 depicts the AA retention in samples 16, 22, and 24 of all drying processes. All AA retentions of MFD are in the range of 86.4% to 99.3%, with most values lying above 90%. CFD shows an AA retention of 88.1% to 94.8%. The ranges of the MFD processes overlap with the CFD range. The only exception is the control concept 1CF, which shows a higher retention of 96.0% to 98.1%. Thus, all MFD processes exhibit high AA retention, comparable to or higher than the retention with CFD. The scattering of AA retention seems to be higher in the individual experimental setups of MFD and CFD than among them. The expected correlation of lower AA retention with higher product temperature was not observed. The detected AA retentions are in a range similar to the values in the literature. AA retentions of approximately 65% to 85% were observed for CFD and MFD of foamed raspberry puree with different formulations at microwave power levels from 1.0 W/g to 2.0 W/g at 0.1 mbar and 30 °C maximum product temperature (Ozcelik et al., 2019). Unblanched potato slices dried at 1.0 mbar showed AA retentions of about 92.5% for CFD at a shelf temperature of 55 °C and 94.4% for MFD with a microwave power of 1.6 W/g (Wang et al., 2010). In contrast, CFD with a maximum product temperature of 55 °C had a notably higher AA retention of 80.3% than the 43.7% observed for MFD with 2 W/g, both at 1.0 mbar (Jiang et al., 2014). These results indicate local overheating during MFD, as observed for foamed raspberry puree at 2 W/g microwave power (Ozcelik et al., 2019).

Regarding the degradation pathway, AA can react reversibly with oxygen to dehydroascorbic acid, which degrades irreversibly to 2,3-diketogulonic acid, followed by further degradation (Szultka et al., 2014). An investigation of the effect of oxygen concentration on the degradation kinetics of AA in malate buffer revealed no influence at temperatures of 50 °C and 60 °C (Gómez Ruiz et al., 2018). At temperatures of 70 °C to 90 °C, however, higher degradation rates were detected with increasing oxygen concentration. These results underline the product-friendly nature of all FD processes investigated with a product temperature below 44.0 °C (compare Section 3.1.2) and the exclusion of oxygen at 0.5 mbar.

3.3. Limitations and future work

The forward power of the SSG was, unfortunately, frequency-dependent. As a result, the forward power could not be kept constant among the control concepts. The variations in forward power were corrected by considering the dissipated power. In future experiments, the forward power should be controlled precisely via a feedback control based on the power emitted to enable direct comparison of all experiments. An additional limitation is the application of different termination criteria for MFD and CFD. While the termination criterion of MFD is based on the weight of the samples, CFD is terminated when all samples have reached their temperature plateau. The solution would be to apply the same termination criterion to both processes, e.g., by means of a comparative pressure measurement (Patel et al., 2010). Note that the temperature measured inside the samples is not the sublimation temperature because a dried layer forms between the fiber optic temperature sensor and the sublimation front during MFD. To evaluate the temperature stresses in more detail, the literature suggests combining the use of marker substances with thermal imaging (Kalinke and Kulozik, 2023).

Regarding product analysis, it must be noted that handling the hygroscopic samples at varying humidity could have influenced the residual moisture. Additionally, the equivalence points for AA retention were detected by visual perception rather than by more precise automated methods and the experimental procedure lasted several hours, which may have caused degradation of AA during the measurements.

Process control strategies based on the control concepts investigated should be transferred to industry-relevant products in future work. The most promising control strategy seems to be the application of RFs with real-time adjustment. In preliminary MFD experiments with potatoes, puffing did not occur under process conditions similar to those in this work. These results suggest that tylose gel might be especially prone to puffing due to the rigid outer layer formed during MFD. Moreover, the investigated control concepts could be refined to shorten the process time or prevent puffing. This might be achieved by using more elaborate algorithms, such as genetic algorithms, or the combination with additional sensor data, like a frequency control based on the recorded product temperature or weight. Future work could also involve incorporating multiple SSGs in the MFD system, enabling the investigation of microwave application with phase shift or simultaneous use of multiple frequencies. Scaling up MFD is another interesting line of work to investigate its competitiveness with CFD and tackle a major challenge to its industrial application. Additionally, hybrid freeze-drying, where energy input from microwaves is combined with conventional heat transfer, could be explored experimentally. This combination could lead to synergistic effects between rapid microwave heating and compensatory thermal heat transfer that cools the samples when their temperature rises above the shelf temperature. Lastly, the underlying control strategies could be transferred to other microwave-assisted processes like heating or defrosting.

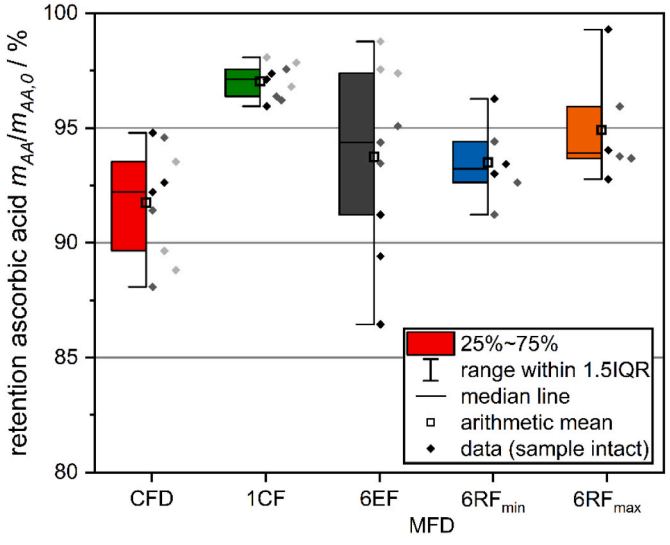

Fig. 10. Ascorbic acid retention of samples 16, 22, and 24 from the conducted experiments in MFD and CFD. The samples of each experiment within the various processes are shown in a different shade of gray.

4. Conclusions

The present work demonstrates the advantages of frequency adjustment during drying for MFD based on feedback related to product state. The application of multiple energy-efficient RFs in the 6RF$_{max}$ control concept resulted in an average energy efficiency of the conversion of electromagnetic energy into heat of 64.63%, which was an increase by an absolute value of 24.51% compared to the application of constant frequencies with 6EF. The highest temperature recorded among all MFD experiments, at 43.8 °C, was comparable to the maximum temperature of 44.0 °C in CFD. The specific forward power in the MFD experiments was frequency-dependent. Therefore, it varied among the control concepts. Nevertheless, the maximum energy efficiency for 6RF$_{max}$ corresponded to the highest average specific dissipated power and, consequently, to the highest drying rate. These process conditions caused a process duration of 11.68 h for MFD with 6RF$_{max}$, a reduction of 24.2% compared to CFD and 38.4% compared to MFD with 6EF. The effects of frequency adjustment on energy efficiency, product temperature, and drying rate were reflected by fluctuations of the

parameters when RFs were adjusted every 20 min.

Similar residual moisture contents and AA retentions compared to CFD were obtained with all MFD control concepts. The product properties fell within the typical range observed for FD of food products, with dry basis residual moisture ranging from 0.002 g/g to 0.029 g/g and AA retention ranging from 86.4% to 99.3%. Structural impairment due to puffing was observed for MFD with all control concepts and affected up to 10.4% of the samples. The number of puffed samples could be reduced by applying frequencies with lower energy efficiency or reducing microwave power. In contrast, no puffing occurred during CFD.

CRediT authorship contribution statement

Till Kaysan: Writing – original draft, Visualization, Validation, Software, Project administration, Methodology, Investigation, Funding acquisition, Formal analysis, Data curation, Conceptualization. **Xiaoqi Zhou:** Writing – review & editing, Visualization, Methodology. **Volker Gaukel:** Writing – review & editing, Supervision, Resources, Project administration, Funding acquisition, Conceptualization.

Declaration of generative AI and AI-assisted technologies in the writing process

While preparing this work, the authors used DeepL to translate it into English. Grammarly, GPT 3.5, and GPT 4o were used to correct spelling and grammar. After using these tools, the authors reviewed and edited the content as needed and take full responsibility for the content of the publication.

Declaration of competing interest

The authors declare that they have no known competing financial interests or personal relationships that could have appeared to influence the work reported in this paper.

Data availability

Data will be made available on request.

Acknowledgments

We thank Prof. Gisela Guthausen from the Institute of Mechanical Process Engineering and Mechanics and Engler-Bunte-Institute of KIT for her support in μ-CT imaging.

This research was funded as an IGF project of the FEI via AiF under the Program for Promoting Industrial Collective Research (IGF) of the German Federal Ministry for Economic Affairs and Climate Action (BMWK), based on a resolution of the German Parliament, Project 22205 N.

Appendix A. Supplementary data

Supplementary data to this article can be found online at https://doi.org/10.1016/j.jfoodeng.2024.112221.

References

Ambros, S., Mayer, R., Schumann, B., Kulozik, U., 2018. Microwave-freeze drying of lactic acid bacteria: influence of process parameters on drying behavior and viability. Innov. Food Sci. Emerg. Technol. 48, 90–98.

Antonio, C., Deam, R.T., 2005. Comparison of linear and non-linear sweep rate regimes in variable frequency microwave technique for uniform heating in materials processing. J. Mater. Process. Technol. 169 (2), 234–241.

Atuonwu, J.C., Tassou, S.A., 2018. Quality assurance in microwave food processing and the enabling potentials of solid-state power generators: a review. J. Food Eng. 234, 1–15.

Ballentine, R., 1941. Determination of ascorbic acid in citrus fruit juices. Ind. Eng. Chem. Anal. Ed. 13 (2), 89.

Bianchi, C., Bonato, P., Dughiero, F., Canu, P., 2017. Enhanced power density uniformity for microwave catalytic reactions adopting solid-state generators: comparison with magnetron technology. Chem. Eng. Process: Process Intensif. 120, 286–300.

Clark, D.E., Sutton, W.H., 1996. Microwave processing of materials. Annu. Rev. Mater. Sci. 26 (1), 299–331.

Drouzas, A., Tsami, E., Saravacos, G., 1999. Microwave/vacuum drying of model fruit gels. J. Food Eng. 39 (2), 117–122.

Dumpler, J., Moraru, C.I., 2023. Microwave vacuum drying of dairy cream: processing, reconstitution, and whipping properties of a novel dairy product. J. Dairy Sci.

Gómez Ruiz, B., Roux, S., Courtois, F., Bonazzi, C., 2018. Kinetic modelling of ascorbic and dehydroascorbic acids concentrations in a model solution at different temperatures and oxygen contents. Food Res. Int. 106, 901–908.

Gulati, T., Datta, A.K., 2016. Coupled multiphase transport, large deformation and phase transition during rice puffing. Chem. Eng. Sci. 139, 75–98.

Härdter, N., Geidobler, R., Presser, I., Winter, G., 2023. Accelerated production of biopharmaceuticals via microwave-assisted freeze-drying (MFD). Pharmaceutics 15 (5).

Hasegawa, Y., Nakamura, K., Lubomirsky, D., Park, S., Kobayashi, S., Sugai, H., 2017. Microwave plasma generation by the fast rotation and slow pulsation of resonant fields in a cylindrical cavity. Jpn. J. Appl. Phys. 56 (4), 46203.

Huang, L., Zhang, M., Mujumdar, A.S., Lim, R.-X., 2011. Comparison of four drying methods for re-structured mixed potato with apple chips. J. Food Eng. 103 (3), 279–284.

Jiang, H., Zhang, M., Liu, Y., Mujumdar, A.S., Liu, H., 2013. The energy consumption and color analysis of freeze/microwave freeze banana chips. Food Bioprod. Process. 91 (4), 464–472.

Jiang, H., Zhang, M., Mujumdar, A.S., Lim, R.-X., 2014. Comparison of drying characteristic and uniformity of banana cubes dried by pulse-spouted microwave vacuum drying, freeze drying and microwave freeze drying. J. Sci. Food Agric. 94 (9), 1827–1834.

Kalinke, I., Kulozik, U., 2023. Irreversible thermochromic ink in the identification of over- and under-processed product segments in microwave-assisted freeze drying. J. Food Eng. 349, 111470.

Kalinke, I., Pusl, F., Häderle, F., Kulozik, U., 2023. A comparative study of frequency-shifting strategies for uniform and energy-efficient microwave heating in solid-state microwave systems. Innov. Food Sci. Emerg. Technol. 86, 103388.

Miyakawa, M., Kanamori, S., Hagihara, K., Itagaki, A., Nakamura, T., Nishioka, M., 2021. Cylindrical resonator-type microwave heating reactor with real-time monitoring function of dielectric property applied to drying processes. Ind. Eng. Chem. Res. 60 (25), 9119–9127.

Ozcelik, M., Heigl, A., Kulozik, U., Ambros, S., 2019. Effect of hydrocolloid addition and microwave-assisted freeze drying on the characteristics of foamed raspberry puree. Innov. Food Sci. Emerg. Technol. 56, 102183.

Patel, S.M., Doen, T., Pikal, M.J., 2010. Determination of end point of primary drying in freeze-drying process control. AAPS PharmSciTech 11 (1), 73–84.

Saguy, I., Kopelman, I.J., Mizrahi, S., 1978. Simulation of ascorbic acid stability during heat processing and concentration of grapefruit juice. J. Food Process. Eng. 2 (3), 213–225.

Shishehgarha, F., Makhlouf, J., Ratti, C., 2002. Freeze-drying characteristics of strawberries. Dry. Technol. 20 (1), 131–145.

Sickert, T., Bergmann, R., Christoph, J., Gaukel, V., 2023a. A time-saving approach to parameter studies in microwave-assisted freeze drying. Processes 11 (10), 2886.

Sickert, T., Kalinke, I., Christoph, J., Gaukel, V., 2023b. Microwave-assisted freeze-drying with frequency-based control concepts via solid-state generators: a simulative and experimental study. Processes 11 (2), 327.

Siebert, T., Zuber, M., Hamann, E., Baumbach, T., Karbstein, H.P., Gaukel, V., 2020. Micro-CT visualization of structure development during freeze-drying processes. Dry. Technol. 38 (3), 376–384.

Straube, C., Meyer, J., Dittler, A., 2021. Identification of deposited oil structures on thin porous oil mist filter media applying μ-CT imaging technique. Separations 8 (10), 193.

Szultka, M., Buszewska-Forajta, M., Kaliszan, R., Buszewski, B., 2014. Determination of ascorbic acid and its degradation products by high-performance liquid chromatography-triple quadrupole mass spectrometry. Electrophoresis 35 (4), 585–592.

Taghian Dinani, S., Feldmann, E., Kulozik, U., 2021. Effect of heating by solid-state microwave technology at fixed frequencies or by frequency sweep loops on heating profiles in model food samples. Food Bioprod. Process. 127, 328–337.

Tang, Z., Hong, T., Liao, Y., Chen, F., Ye, J., Zhu, H., Huang, K., 2018. Frequency-selected method to improve microwave heating performance. Appl. Therm. Eng. 131 (2), 642–648.

Thostenson, E.T., Chou, T.-W., 1999. Microwave processing: fundamentals and applications. Compos. Part A Appl. Sci. Manuf. 30 (9), 1055–1071.

Tsubaki, S., Nakasako, Y., Ohara, N., Nishioka, M., Fujii, S., Wada, Y., 2020. Ultra-fast pyrolysis of lignocellulose using highly tuned microwaves: synergistic effect of a cylindrical cavity resonator and a frequency-auto-tracking solid-state microwave generator. Green Chem. 22 (2), 342–351.

Wang, R., Zhang, M., Mujumdar, A.S., 2010. Effects of vacuum and microwave freeze drying on microstructure and quality of potato slices. J. Food Eng. 101 (2), 131–139.

Wang, W., Zhao, C., Sun, J., Wang, X., Zhao, X., Mao, Y., Li, X., Song, Z., 2015. Quantitative measurement of energy utilization efficiency and study of influence factors in typical microwave heating process. Energy 87, 678–685.

Yang, F., Wang, W., Yan, B., Hong, T., Yang, Y., Zhu, H., Wu, L., Huang, K., 2019. Sweep frequency heating based on injection locked magnetron. Processes 7 (6), 341.

Yang, R., Chen, J., 2022. Dynamic solid-state microwave defrosting strategy with shifting frequency and adaptive power improves thawing performance. Innov. Food Sci. Emerg. Technol. 81, 103157.
Yang, R., Fathy, A.E., Morgan, M.T., Chen, J., 2022a. Development of a complementary-frequency strategy to improve microwave heating of gellan gel in a solid-state system. J. Food Eng. 314, 110763.
Yang, R., Fathy, A.E., Morgan, M.T., Chen, J., 2022b. Development of online closed-loop frequency shifting strategies to improve heating performance of foods in a solid-state microwave system. Food Res. Int. 154, 110985.
Yang, R., Morgan, M., Fathy, A., Luckett, C., Wang, Z., Chen, J., 2023. A comprehensive evaluation of microwave reheating performance using dynamic complementary-frequency shifting strategy in a solid-state system. Food Bioprocess Technol. 16 (5), 1061–1075.
Zhou, X., Tang, Z., Pedrow, P.D., Sablani, S.S., Tang, J., 2023. Microwave heating based on solid-state generators: new insights into heating pattern, uniformity, and energy absorption in foods. J. Food Eng. 357, 111650.
Zhou, X., Zhang, S., Tang, Z., Tang, J., Takhar, P.S., 2022. Microwave frying and post-frying of French fries. Food Res. Int. 159, 111663.
Zou, K., Teng, J., Huang, L., Dai, X., Wei, B., 2013. Effect of osmotic pretreatment on quality of mango chips by explosion puffing drying. LWT 51 (1), 253–259.